

Regioselective *ortho* Amination of Coordinated 2-(Arylazo)pyridine. Isolation of Monoradical Palladium Complexes of a New Series of Azo-Aromatic Pincer Ligands

Debabrata Sengupta,[†] Nabanita Saha Chowdhury,[†] Subhas Samanta,^{†,◇,#} Pradip Ghosh,[†] Saikat Kumar Seth,[§] Serhiy Demeshko,[#] Franc Meyer,[#] and Sreebrata Goswami^{*,†}

[†]Department of Inorganic Chemistry, Indian Association for the Cultivation of Science, Jadavpur, Kolkata 700 032, India

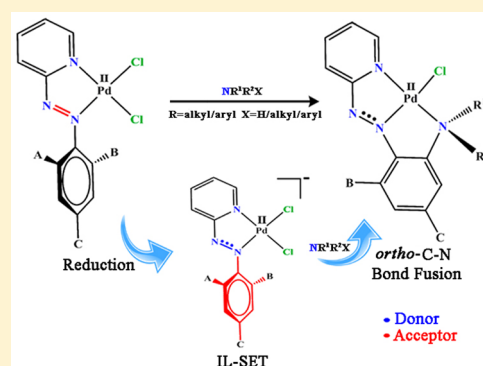
[◇]Department of Chemical Sciences, Indian Institute of Science Education and Research Kolkata, Mohanpur 741246, Nadia, India

[#]Institut für Anorganische Chemie, Georg-August-Universität Göttingen, Tammannstraße 4, 37077 Göttingen, Germany

[§]Department of Physics, Mugberia G. Mahavidyalaya, Bhupatinagar, Purba Medinipur 721425, India

S Supporting Information

ABSTRACT: In an unusual reaction of $[\text{Pd}(\text{L}^1)\text{Cl}_2]$ ($\text{L}^1 = 2\text{-(arylazo)pyridine}$) with amines, a new series of palladium complexes $[\text{Pd}(\text{L}^{2\bullet-})\text{Cl}]$ ($\text{L}^2 = 2\text{-}((2\text{-amino)arylazo)pyridine}$) (**1a–1h**) were isolated. The complexes were formed via N–H and N–C bond cleavage reactions of 1°/2° and 3° amines, respectively, followed by regioselective aromatic *ortho*-C–N bond formation reaction and are associated with *ortho*-C–H/*ortho*-C–Cl bond activation. A large variety of amines including both aromatic and aliphatic were found to be effective in producing air-stable complexes. Identity of the resultant complexes was confirmed by their X-ray structure determination. Efforts were also made to understand the mechanism of the reaction. A series of experiments were performed, which point toward initial ligand reduction followed by intraligand electron transfer. Examination of the structural parameters of these complexes (**1**) indicates that the in situ generated ligand coordinated to the Pd^{II} center serves as the backbone of these air-stable monoradical complexes. Molecular and electronic structures of the isolated complexes were further scrutinized by various spectroscopic techniques including cyclic voltammetry, variable temperature magnetic susceptibility measurements, electron paramagnetic resonance, and UV–vis spectroscopy. Finally the electronic structure was confirmed by density functional theory calculations. The isolated monoradical complexes adopt an unusual π -stacked array, which leads to a relatively strong antiferromagnetic interaction ($J = -40 \text{ cm}^{-1}$ for the representative complex **1c**).



INTRODUCTION

Events associated with transition metal complexes containing redox active ligands have attracted considerable interest in recent times.¹ Research in this area is encouraged by, inter alia, various metalloenzymatic transformations where ligand-radical containing intermediates were found to be active species that enable unusual reactivity.² Moreover such complexes can also show interesting magnetic properties³ as well as memory device applications.⁴ Very recently, it has been argued that transition metal coordinated redox active ligands can also act as source or sink of electrons in metal complex mediated/catalyzed transformations.⁵ For example, pioneer works of Wieghardt and Chirik on redox active ligand-containing complexes catalyzed reactions are prominent examples where ligand redox is used in bond-breaking and bond-making processes.^{1a,6}

Recently van der Vlugt et al. reported⁷ an example of a palladium complex where ligand-to-substrate single electron transfer (SET) is involved in chemical reactions. Herein we report the reactivity of a series of redox-active azo-aromatic palladium complexes where intraligand single electron transfer

(IL-SET) between two nonconjugative counterparts of a coordinated azoaromatic ligand (L^1) is operative behind a regioselective *ortho*-C–N bond formation reaction. Ligand-radical mediated SET reactivity has been recently identified and is a rarely observed phenomenon in transition metal complex mediated organic transformations.^{6c,7,8}

While working on redox-active azo-aromatic ligands, previously we observed⁹ that primary aromatic amines react with metal coordinated 2-(arylazo)pyridine ligands freely to give complexes of monoanionic tridentate NNN donor ligands (Scheme 1). However, these reactions were limited only to primary aromatic amines, and our attempts to achieve similar reactivity with 2° and 3° aromatic as well as aliphatic amines were unsuccessful.

Here, in an attempt to isolate a homoleptic palladium complex, we observe an unusual aromatic C–N bond formation reaction with a large variety of both aromatic and

Received: September 12, 2015

Table 1. Products of the Regiospecific *ortho*-C–N Coupling Reaction on Coordinated Azo-Aromatic Ligand with Amines

ligand(L ¹)		NR ¹ NR ² X			AX/BX	ligand(L ²)	compound
		R ¹	R ²	X			
A = H	L ^{1a}	Me	Me	H, Me	H ₂ /CH ₄	L ^{2a}	1a
B = H		Et	Et	H, Et	H ₂ /C ₂ H ₆	L ^{2b}	1b
C = H		Me	Ph	H	H ₂	L ^{2c}	1c
A = H	L ^{1b}	Me	Me	H, Me	H ₂ /CH ₄	L ^{2d}	1d
B = H		Et	Et	H, Et	H ₂ /C ₂ H ₆	L ^{2e}	1e
C = Cl		Me	Ph	H	H ₂	L ^{2f}	1f
		Ph	Ph	H, Ph	H ₂ /C ₆ H ₆	L ^{2g}	1g
A = Cl	L ^{1c}	Me	Me	H, Me	H ₂ /CH ₄	L ^{2h}	1h
B = H							
C = H							
A = Cl	L ^{1d}	Me	Me	H, Me	HCl/CH ₃ Cl	L ^{2h}	1h
B = Cl							
C = H							
A = H	L ^{1e}	Me	Me	H, Me		NR ^a	
B = H							
C = CH ₃							
A = CH ₃	L ^{1f}	Me	Me	H, Me		NR ^a	
B = CH ₃							
C = H							
A = H	L ^{1a}	H	Ph	H	H ₂	L ^{3a}	1i
B = H							
C = H							

^aNR: No reaction at 50°C; 1i is a nonradical complex, see later.

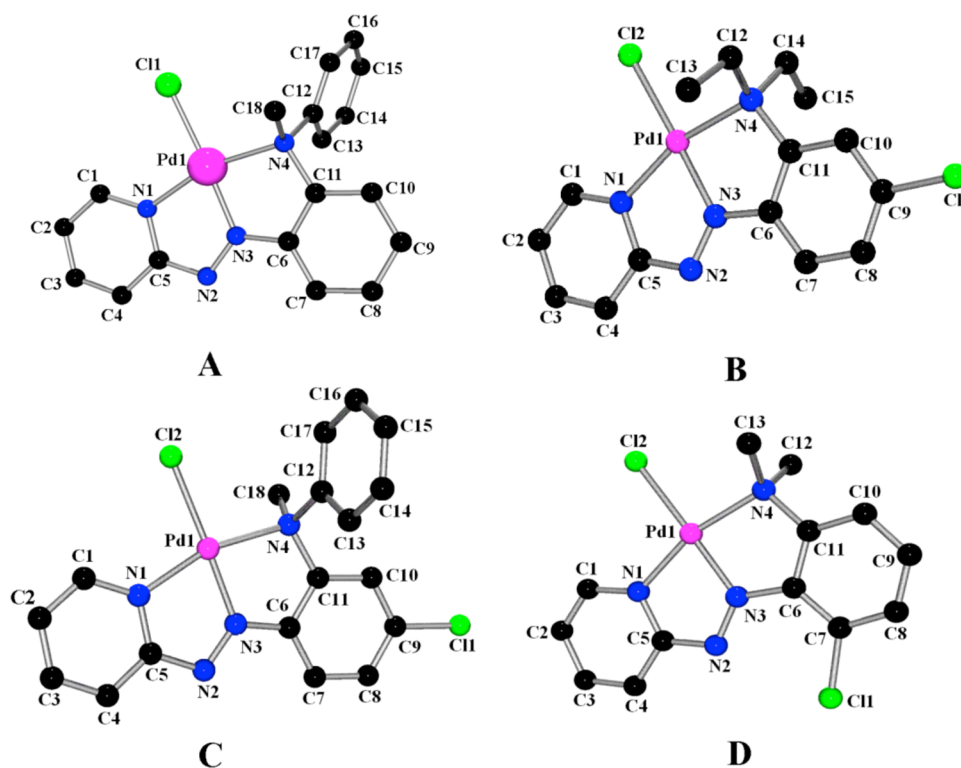


Figure 1. View of the molecular structures of complexes (A) 1c, (B) 1e, (C) 1f, and (D) 1h (Hydrogen atoms are omitted for clarity).

1f, and 1h. Their molecular structures indeed support the chemical reaction depicted in Scheme 2. Views of these complexes are shown in Figure 1. Structural features of all these are more or less similar, and we will use the structure of 1c (Table 2) for our discussion, while details of the other three are submitted as Supporting Information materials (Figures S3–S6

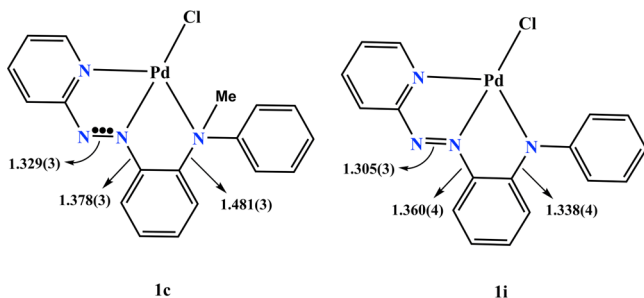
and Tables S5–S6). Here, two major issues emerged: first, the structural analysis confirms the formation of the compounds from the reference chemical reaction; second, there is a considerable elongation of the N2–N3 bond ($d_{\text{N2–N3}} = 1.329(3) \text{ \AA}$), which indicates azo-anion radical character of the coordinated ligand and is consistent with the magnetic

Table 2. Selected Experimental and Calculated Bond Distances (Å) for the Complex **1c**

bond parameters	experimental (1c)	calculated		
		1c ($S = 1/2$)	$[\mathbf{1c}]^+$ ($S = 0$)	$[\mathbf{1c}]^-$ ($S = 0$)
Pd1–Cl1	2.3219(9)	2.362	2.308	2.430
Pd1–N1	2.004(2)	2.033	2.054	2.018
Pd1–N3	1.9197(18)	1.956	1.960	1.958
Pd1–N4	2.100(2)	2.165	2.134	2.211
N2–N3	1.329(3)	1.324	1.269	1.379
N3–C6	1.378(3)	1.381	1.405	1.352
C11–N4	1.481(3)	1.489	1.487	1.488

properties as well as EPR spectra of the complexes (see below). The effects of $d_{\text{N–N}}$ bond elongation of the coordinated ligands in the present complexes are also reflected by the lowering of vibrational frequencies $\nu_{\text{N=N}}$ as compared to uncoordinated L^{3a} . The $\nu_{\text{N=N}}$ band in free L^{3a} appears at $\sim 1380\text{ cm}^{-1}$, whereas those in the present complexes (**1c**) are considerably lower appearing near 1303 cm^{-1} .

It is worth comparing the structure of **1c** with the previously reported palladium complex **1i**.¹⁰ The protonated ligand HL^3 was obtained by a cobalt mediated *ortho*- C_{arom} -amine bond fusion reaction between coordinated L^1 and ArNH_2 . The complex is nonradical with $S = 0$ ground state and its N–N bond is considerably shorter than that in the present radical complexes. Relevant bond lengths of **1c** and **1i** are compared in Scheme 3. It reveals that $d_{\text{N–N}}$ in the former is considerably

Scheme 3. Comparison of Bond Lengths of the Two Related Complexes **1c** and **1i**^a

^a**1c**: neutral NNN donor tridentate ligand complex, **1i**: monoanionic NNN donor tridentate ligand complex.

elongated compared to the later. Moreover C–N lengths on either side of the central *o*-phenylene ring in these two complexes are also quite different. Bond length contraction of these two bonds in the complexes of the anionic ligand has been attributed to delocalization of negative charge along the ligand backbone. However, such delocalization is expected to be absent^{9a} in the azo-anion radical complexes. Thus, the above two examples of Pd^{II} complexes have provided a direct experimental evidence that neutral azoaromatic donors¹³ are far more promising candidates for sequential redox events than the corresponding anionic ligands.

Intermolecular Interaction and Magnetic Properties.

Detailed examination of the crystal structure of complex **1c** shows that the metal center is displaced by 0.028 Å out of the least-squares planes defined by the donor atoms. The ligand forms two five-membered chelate rings, and the dihedral angle between the two related mean ring planes is 0.92° . In **1c**, the

C(6) and N(3) atoms have the largest deviations in opposite directions [C(6): $+0.025(2)\text{ Å}$, N(3): $-0.023(2)\text{ Å}$] from the least-squares mean plane through the atoms N(1)–C(5)–N(2)–N(3)–C(6)–C(11)–N(4)–Pd(1). In the solid state, the structure is stabilized through intermolecular C–H \cdots Cl, C–H \cdots π , and π – π stacking interactions (Tables S7 and S8). The methyl carbon atom C(18) in the molecule at (x, y, z) acts as donor to the Cl(1) in the molecule at $(1/2 - x, -1/2 + y, 1/2 - z)$. The aryl ring carbon atom C(14) is in contact with the ring centroid of another aryl ring C(6)–C(11) through C–H \cdots π stacking interactions (Figure S7), thus generating a dimeric unit through C–H \cdots π interactions.¹⁴ Because of their self-complementary nature, the molecules are juxtaposed via face-to-face π -stacking interactions.¹⁵ The pyridine rings N(1)/C(1)–C(5) of the molecules at (x, y, z) and $(1 - x, 1 - y, 1 - z)$ are strictly parallel, with an interplanar spacing of $4.018(2)\text{ Å}$ and a ring centroid separation of $4.128(2)\text{ Å}$, corresponding to a ring offset of 0.948 Å . The mutual influence of the C–H \cdots π bonds and face-to-face π -stacking interactions between the pyridine rings led the molecules to build a two-dimensional supramolecular assembly in the $(1\ 0\ 1)$ plane (Figure S8). In another substructure, the molecular packing is such that the π – π stacking interactions between the pyridine rings of adjacent partner molecules are optimized. These pyridine rings are also in contact with the centroids of the aryl ring C(6)–C(11) with an intercentroid distance of $3.840(2)\text{ Å}$ and interplanar spacing of $3.306(2)\text{ Å}$. Thus, the mutual influence of the two types of π – π stacking interactions leads the molecules to propagate into a supramolecular layered assembly in the $(1\ 1\ 0)$ plane (Figure 2).

These intermolecular interactions in solid state prompted us to investigate the variable-temperature magnetic behavior, again using **1c** as a representative example. Magnetic measurements were performed using polycrystalline material of **1c** in a SQUID magnetometer in the temperature range of 2 – 295 K (Figure 3). The $\chi_M T$ value per dimeric unit at room temperature is $\sim 0.64\text{ cm}^3\text{ mol}^{-1}\text{ K}$, corresponding to an effective magnetic moment of $2.26\mu_B$. This value is lower than the expected spin-only value of $0.75\text{ cm}^3\text{ mol}^{-1}\text{ K}$ (or $2.45\mu_B$) for two uncoupled ions with $S = 1/2$. On lowering the temperature to 2 K , $\chi_M T$ tends to zero, indicating a singlet ground state ($S = 0$). The experimental data were fitted using the appropriate Heisenberg–Dirac–van Vleck spin Hamiltonian that includes isotropic exchange coupling and Zeeman splitting, (eq 1).

$$\hat{H} = -2J\hat{S}_1\hat{S}_2 + g\mu_B\vec{B}(\vec{S}_1 + \vec{S}_2) \quad (\text{eq 1})$$

The best fit parameters are $g = 1.99$ and $J = -40.2\text{ cm}^{-1}$. Better agreement with experimental data was obtained when additional intermolecular interactions were considered in a mean field approach by using a Weiss temperature Θ . This parameter $\Theta = -15.2\text{ K}$ relates to the intermolecular interactions of $zJ_{\text{inter}} = -42.3\text{ cm}^{-1}$, where J is the interaction parameter between two nearest neighbor magnetic centers and z is the number of nearest neighbors. On the basis of the structural information, three pathways for the exchange interactions can be considered. Two of them may result from the two different kinds of π – π stacking interactions with corresponding distances of 3.840 and 4.128 Å (Figure 2); the third pathway may arise through the C–H \cdots π hydrogen bond interactions (Figure S7). According to the spin density distribution from density functional theory (DFT) calculations

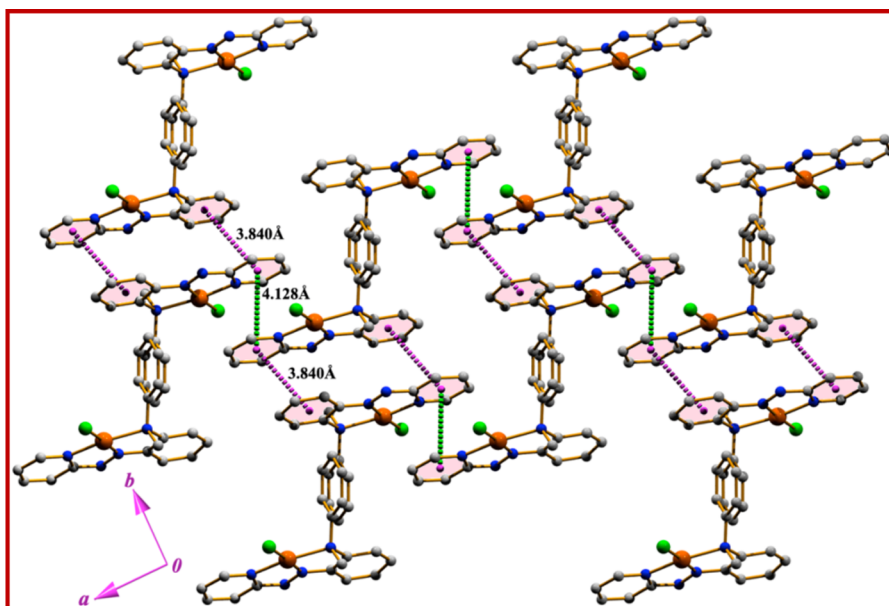


Figure 2. Supramolecular layer architecture in the complex **1c** assembled through cooperative π - π stacking interactions.

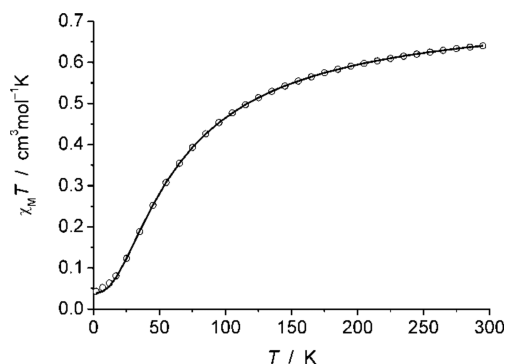


Figure 3. $\chi_M T$ vs T plot for complex **1c**, calculated for a dimeric motif. The solid line represents the best fit curve.

(see below), the unpaired electron is delocalized over the backbone of the ligand, that is, into the pyridine and aryl rings that form the five-membered chelate rings, whereas no spin density is present on the phenyl rings involved in C-H \cdots π hydrogen bond interactions. Therefore, the coupling $J = -40.2$ cm^{-1} can be attributed to the shorter π - π stacking interactions of 3.840 Å, while weaker intermolecular interactions $zJ_{\text{inter}} = -42.3$ cm^{-1} (or $J_{\text{inter}} = -21.2$ cm^{-1} for the case $z = 2$) should arise from π - π stacking interactions with longer distances of 4.128 Å. In general, the strength of the magnetic exchange interaction in the π - π stacking systems depends on the spin density on the interacting atoms as well as on the contact distances and can vary from fractions of one wavenumber up to extremely strong (larger than -1000 cm^{-1}) coupling.¹⁶ The observed coupling constant of -40.2 cm^{-1} in **1c** with the vertical distances from ring centroids to rings of 3.31 to 3.39 Å (Table S8) is comparable with literature data for systems with similar metric parameters. For example, coupling constants of -58 cm^{-1} or -52 cm^{-1} were observed for the verdazyl radical with interplanar spacing of 3.37 and 3.44 Å, or for phenylene-based radicals with the closest C \cdots C distances between phenalenyl units of 3.54 to 3.66 Å, respectively.¹⁷

Electrochemistry and Density Functional Theory. The Pd complexes (**1a–h**) showed a reversible one-electron

oxidation near 0.25 V and another one-electron reversible reduction near -0.7 V. Cyclic voltammetry data of all complexes are collected in the Supporting Information (Table S2 and Figures S9–S15), and that of a representative complex **1c** is shown in Figure 4. The corresponding nonradical

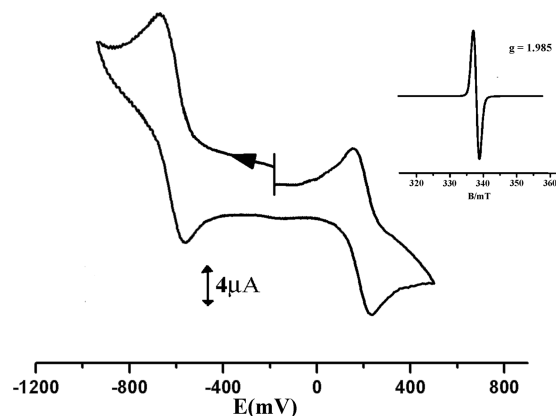


Figure 4. Cyclic voltammogram of complex **1c** (in $\text{CH}_2\text{Cl}_2/0.1$ M Bu_4NClO_4 , scan rate 50 mV/s; potentials vs SCE). (inset) EPR spectrum (X-band) of the complex **1c** at 120 K in dichloromethane-toluene glass.

complex, $[\text{Pd}(\text{L}^{3a})\text{Cl}]$ (**1i**), showed¹² one reversible azo-based reduction at -0.2 V and an ill-defined oxidative wave at higher anodic potentials. The nature of the redox processes in the representative complex **1c** was studied by DFT calculations.

To have a closer look into the electronic structure of the complexes, we performed a series of calculations using DFT (B3LYP; see Supporting Information for details). The computed metric parameters of the complex **1c** are in reasonable agreement with the experimentally observed parameters. A spin density plot for **1c**, shown in Figure 5, indicates almost one-electron spin delocalization over the ligand backbone (96% on L^2 and 4% on Pd) signifying that the unpaired spin resides almost exclusively on the coordinated ligand, which is well-consistent with the aforementioned exper-

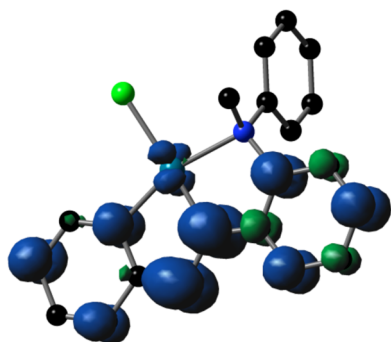
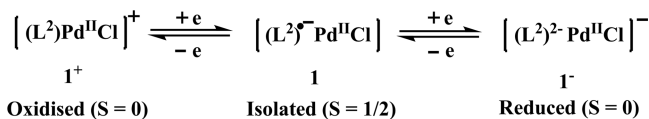


Figure 5. Spin-density plot for **1c** derived from DFT calculations.

imental findings. Comparison of calculated structural parameters between **1c** and its corresponding one-electron oxidized complex reveals a contraction of the azo bond length ($d_{N2-N3} \approx 1.269$ Å in [**1c**]⁺). Our attempts to isolate the oxidized complex [**1c**]⁺ were unsuccessful. However, the complex [**1f**]⁺ shows an $S = 0$ ground state, as evidenced by its ¹H NMR spectrum with resonances appearing in the normal range of diamagnetic compounds (see Supporting Information Figure S16). The complex **1f** is identical in all respects to **1c** with the only difference that the ligand here is chloro-substituted. It is therefore concluded that the oxidation of **1c** is also ligand-centered. The reduction of **1c** is identified to impart a single-bond character to the N(2)–N(3) bond (ca. 1.379 Å). A comparison of calculated bond lengths in the Pd complexes is tabulated in Table 2. Notably, the lowest unoccupied molecular orbital (LUMO) in **1c**⁺ is localized over the π^* azo orbital of the azo-function, while the highest occupied molecular orbital (HOMO) in the reduced complex, **1c**[−] is distributed over the ligand containing azo-function, which indicates that the redox processes occurred exclusively at the ligand (Figure S22).

With all these results taken together, it is concluded that redox events in the Pd complexes occur at the ligand without affecting the bivalent oxidation state of metal. Thus, the redox processes in these complexes involve the following three redox states (Scheme 4).

Scheme 4. Electron-Transfer Series for Complexes **1a–h**



The radical complexes are intensely blue-violet colored and showed multiple transitions in the optical spectral range, from 250 to 800 nm (Supporting Information Figure S17). For example, the complex **1c** has two broad bands at 575 and 348 nm. Upon oxidation the broad band at 575 nm slightly shifted to 580 nm. However, upon reduction this band shifts to a shorter wavelength 506 nm. To assign the electronic transition, TD-DFT calculations were performed on three states of the complex, specifically, **1c**, [**1c**]⁺, and [**1c**][−]. Good agreement between computed absorption spectra and the experimentally observed ones was noted. For example, in the case of **1c** the computed absorption at 511 nm (HOMO(β) \rightarrow LUMO(β)) is in reasonable agreement with the experimentally observed band at 575 nm, where both HOMO(β) and LUMO(β) orbitals are localized on the ligand.

Thus, this absorption is assigned to an intraligand transition. The computed one-electron oxidized complex showed a HOMO to LUMO transition at 596 nm that appeared at 580 nm in the experimentally observed spectrum. The HOMO is localized over the *N*-phenyl ring, whereas the LUMO is concentrated on the N=N π^* array. The broad transition at 506 nm for the one-electron reduced species corresponds well to the computed HOMO to LUMO+1 transition at 459 nm. The experimentally observed spectra are shown in Figure 6, and associated orbitals are tabulated in Table S3.

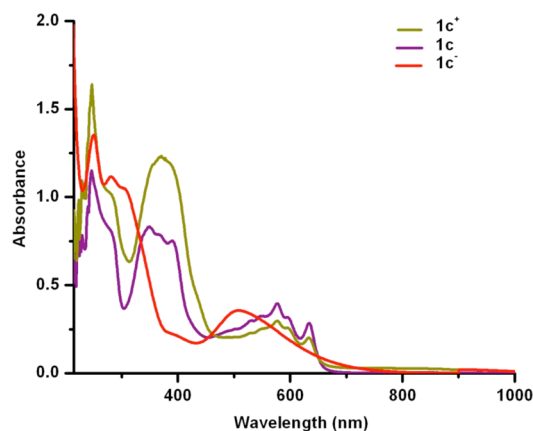


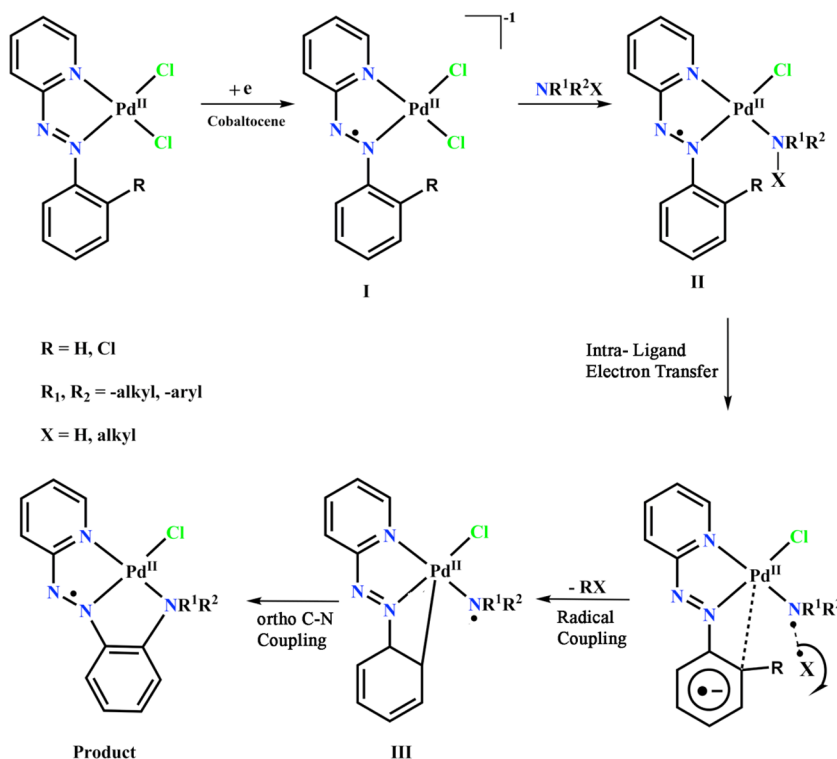
Figure 6. Electronic spectra of **1c** (violet) and coulometrically generated [**1c**]⁺ (dark yellow) and [**1c**][−] (red) in dichloromethane solution.

Mechanistic Investigations. To gain insight into the aromatic ring amination reaction the following experiments were planned. First we checked the reactivity of the complex with different quantities of cobaltocene, CoCp₂, with respect to the starting palladium complex. It is found that the reaction occurs even in the presence of 0.25 equiv of CoCp₂. However, maximum yields of the products were obtained when equimolar quantities of [Pd(L¹)Cl₂] and CoCp₂ were used. We thus propose that single-electron reduction of the palladium complex is needed for this reaction to occur. Moreover, it was noted before that with less reducing amines such as 1° and 2° amines the reactions do not occur at all without an external reductant. It is thus believed that formation of the one-electron reduced ligand radical complex^{11a} (**I**) is the initial step for the reaction as shown in Scheme 5.

The formation of the one-electron reduced complex was further supported by EPR spectroscopy and mass spectrometry (MS). For example, the isolated one-electron reduced species [Pd(L^{1b})Cl₂][−] gives a single-line EPR signal at $g = 1.99$ characteristic for a ligand-centered radical, and a molecular ion peak at $m/z = 392.72$ amu in negative ion mode electrospray ionization (ESI) MS, which matches well with the formulation of the intermediate **I** (Supporting Information Figures S18 and S19). Our attempts to characterize the reduced complex by IR spectroscopy shows that $\nu_{N=N}$ shifts from 1413 cm^{−1} [in Pd(L^{1a})Cl₂] to 1340 cm^{−1} in the reduced complex, indicating primarily azo-reduction.

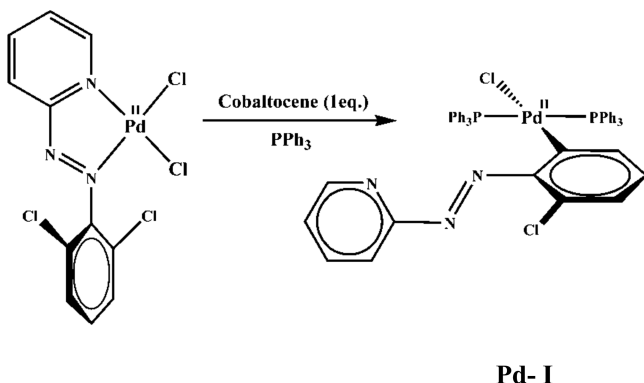
The idea that the reaction goes through a radical intermediate was further corroborated by the fact that it is completely ceased in the presence of a radical scavenger like 2,2,6,6-tetramethylpiperidinoxyl radical or 2,6-di-*tert*-butyl-4-methylphenol. Notably, it is known that upon ligand reduction of a transition metal complex bearing redox noninnocent

Scheme 5. Plausible Reaction Mechanism



ligands, the lability of the ligand in the reduced complex increases substantially.¹⁸ Thus, we anticipate that one of the chloride ligands becomes labile in $[\text{Pd}(\text{L}^1)\text{Cl}_2]^-$ and is subsequently replaced by the incoming neutral amine to form¹⁹ the intermediate radical complex II as shown in Scheme 5. We have not yet been successful to isolate such an intermediate complex with amines; however, a similar reaction in the presence of triphenylphosphine (PPh_3) leads to the isolation of a new complex, Pd-I, confirming the lability of one of the Cl^- ligands. (Scheme 6 and Figure 7).

Scheme 6



Notably, a similar reaction of PPh_3 with the parent complex $[\text{Pd}(\text{L}^1)\text{Cl}_2]$ does not show any substitution reaction. Now the intermediate ligand radical complex is assumed to potentially follow three different types of electron transfer processes for the said chemical reactions: (i) delocalization of the unpaired electron throughout the ligand backbone followed by C–N bond formation, (ii) electron transfer from the radical ligand to

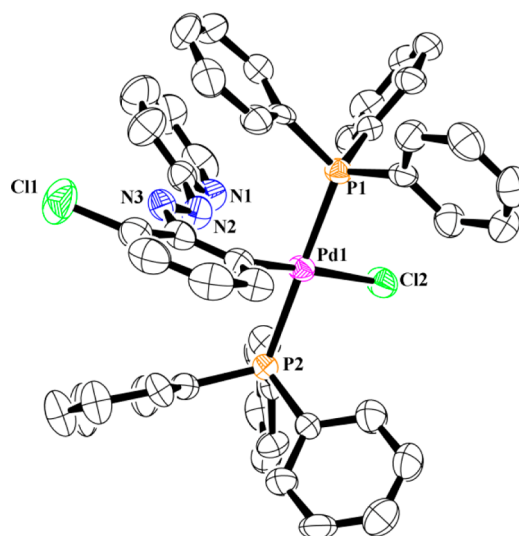
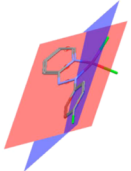
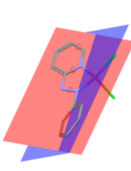
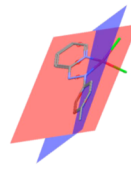
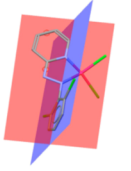
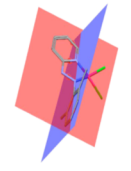
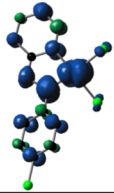
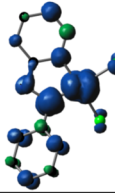
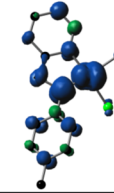
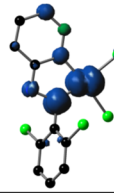
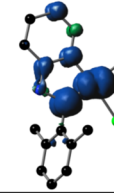


Figure 7. ORTEP representation of the isolated palladium complex (Pd-I) in the presence of PPh_3 at 50% probability ellipsoid (Hydrogen atoms are omitted for clarity).

the incoming amine substrate generating an intermediate radical complex associated with C–N bond formation, (iii) intraligand electron transfer from the π^* -azo to the π^* -phenyl ring in the ligand associated with C–N bond formation reaction.

The phenomenon of delocalization of electronic spin along a ligand backbone is implicated in the most frequently observed electron transfer reactivity.²⁰ However, for such a phenomenon planarity of the ligand backbone is essential.²¹ Better delocalization of the electron increases unpaired spin in the reaction center and thus leads to enhanced reactivity. In our case it is evident that the pendant phenyl ring of the ligand L^1 is

Scheme 7. Dihedral Angle between the Ligand Planes and Spin-Density Plots of the Optimized Structures of $[\text{Pd}(\text{L}^1)\text{Cl}_2]^-$

Dihedral angle between two planes in $[\text{Pd}(\text{L}^1)\text{Cl}_2]^-$				
L^{b}	L^{a}	L^{c}	L^{d}	L^{f}
				
28.22°	32.71°	32.74°	64.09°	73.54°
Spin density plots				
				

significantly out of plane from the azo pyridine moiety of the ligand L^1 . For example, the dihedral angle between the planes of the two nonconjugative parts of the ligands is as follows: L^{b} (28.22°), L^{a} (32.71°), L^{c} (32.74°), L^{d} (64.09°), L^{f} (73.54°) (Scheme 7). Thus, introduction of bulky substituents at the *ortho* position increases the dihedral angle. Accordingly the localization of the unpaired spin on the pendent aryl ring decreases as shown in Scheme 7. Thus, it is expected that $[\text{Pd}(\text{L}^{\text{d}})\text{Cl}_2]$ should be the least reactive system in this series. However, in contrast, $[\text{Pd}(\text{L}^{\text{d}})\text{Cl}_2]$ was shown experimentally to have the highest tendency for C–N bond formation reaction. Thus, the argument of C–N bond formation occurring as a result of electron delocalization along the ligand backbone is not valid, and an alternative mechanistic scenario must be operative.

The second possibility involves electron transfer from the reduced ligand to the incoming substrate. Radical ligand-to-substrate electron transfer reactivity is well-documented^{1a,c} in literature in a series of transformations catalyzed by redox-active transition metal complexes. Thus, in our case one may expect electron transfer from a reduced azo-aromatic ligand in the palladium complex to the incoming amine, generating a radical intermediate complex followed by the aforementioned C–N bond formation reaction. Notably, examination of the rates of reactions indicates that the reaction rate is greatly influenced by the substitution on the pendant aryl ring of the ligand L^1 in the complex $[\text{Pd}(\text{L}^1)\text{Cl}_2]$. Such observation may suggest that the elimination step is associated with the rate-limiting step of the reaction. These reactions will involve either formal H_2 or HCl elimination in case of L^1 ligands with at least one H atom in *ortho* position (i.e., one *ortho* position unsubstituted in ligands L^{a} , L^{b} , or L^{c}) or with chloro substituents in both *ortho* positions (ligand L^{d}), respectively, with 1°/2° amines. Corresponding reactions with 3° amines will result in alkane and alkyl/aryl halides, respectively. GC-MS characterization of the crude reaction mixture indeed reveals the elimination of chlorobenzene from the reaction of $[\text{Pd}(\text{L}^{\text{d}})\text{Cl}_2]$ and triphenylamine (supporting Figure S20). Now at this stage we thought of comparing the reaction rates between the two monochloro-substituted complexes, namely, $[\text{Pd}(\text{L}^{\text{b}})\text{Cl}_2]$, $[\text{Pd}(\text{L}^{\text{c}})\text{Cl}_2]$ and the secondary amine Me_2NH . The reaction rates are similar and yielded the products **1d** and **1h**, respectively. This result indicates that H^\bullet elimination is

more facile than Cl^\bullet elimination. Given this result, we planned to examine a similar reaction with a dichloro-substituted complex, $[\text{Pd}(\text{L}^{\text{d}})\text{Cl}_2]$. We anticipated that the reaction rate in this case will be slower than the previous reactions of $[\text{Pd}(\text{L}^{\text{b}})\text{Cl}_2]/[\text{Pd}(\text{L}^{\text{c}})\text{Cl}_2]$ as C–Cl activation is more difficult than C–H activation reaction. However, it is found that in case of $[\text{Pd}(\text{L}^{\text{d}})\text{Cl}_2]$, the reaction rate is faster than the reaction of $[\text{Pd}(\text{L}^{\text{b}})\text{Cl}_2]/[\text{Pd}(\text{L}^{\text{c}})\text{Cl}_2]$, and the product is **1h**. The decreasing order of the reaction rates with the series of different ligands is as follows: $\text{L}^{\text{d}} > \text{L}^{\text{c}} \approx \text{L}^{\text{b}} > \text{L}^{\text{a}} > \text{L}^{\text{e}} > \text{L}^{\text{f}}$. Thus, a comparison of reaction rates in a series of substituted ligands (L^1) did not follow the anticipated trend, as per the previous arguments. Thus, the scenario of initial electron transfer from the reduced azo ligand to the amine substrate associated with C–N bond formation is unlikely.

Then we examine the third possibility of an intraligand electron transfer²² in L^1 for the above reaction. Here, we assume that the reduced azo chromophore in the ligand transfers electron from π^* -azo (singly occupied molecular orbital (SOMO)) to the π^* -orbital (LUMO) of the pendant aryl ring of the ligand. Such electron transfer possibility has also been noted previously for azoaromatic systems, by us²³ as well as by others.⁷ Examination of the MOs of the reduced complex $[\text{Pd}(\text{L}^{\text{a}})\text{Cl}_2]$ shows that the LUMO and LUMO+1 of the complex are close lying and are significantly localized on the pendant phenyl ring of the ligand L^{a} . Localization of these MOs on the pendent aryl ring are expected to be controlled by the substitution on this ring and will be enhanced in case of electron-withdrawing substituent(s). Thus, in the complexes of chloro-substituted ligand LUMO and LUMO+1 are localized primarily on the pendent aryl ring. In contrast, in the case of electron-donating substituted ligand like 4-methyl/2,6-dimethyl groups on the pendent aryl ring, localization becomes more prominent on the azo function as well as on the pyridine ring. Time-dependent (TD) DFT calculation of each of the complexes shows that the SOMO to LUMO and LUMO+1 transition occurs at ~550 to 600 nm, which matches well with the experimental data. For example, experimentally this appears at ~500–650 nm (Table S4 and Figure S21). It may be noted here that this value gradually shifts to higher wavelengths with the introduction of electron-withdrawing substituent and shifts to shorter wavelength by the introduction of electron-donating groups on the pendent aryl ring. Such a change indicates

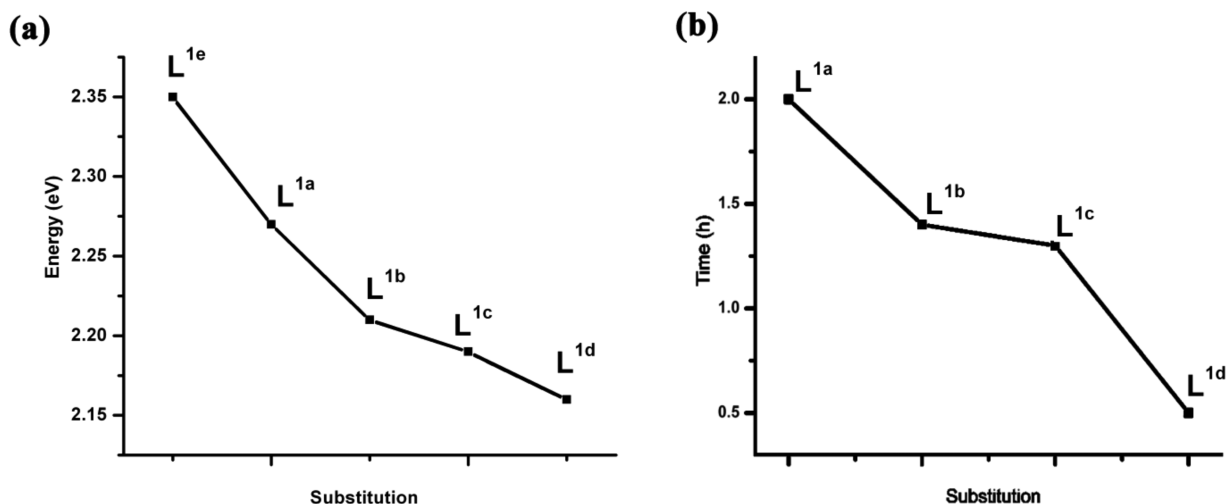


Figure 8. Plot of (a) Experimentally observed SOMO → LUMO/LUMO+1 transition energy with different substituents. (b) Reaction completion time for different ligands L¹.

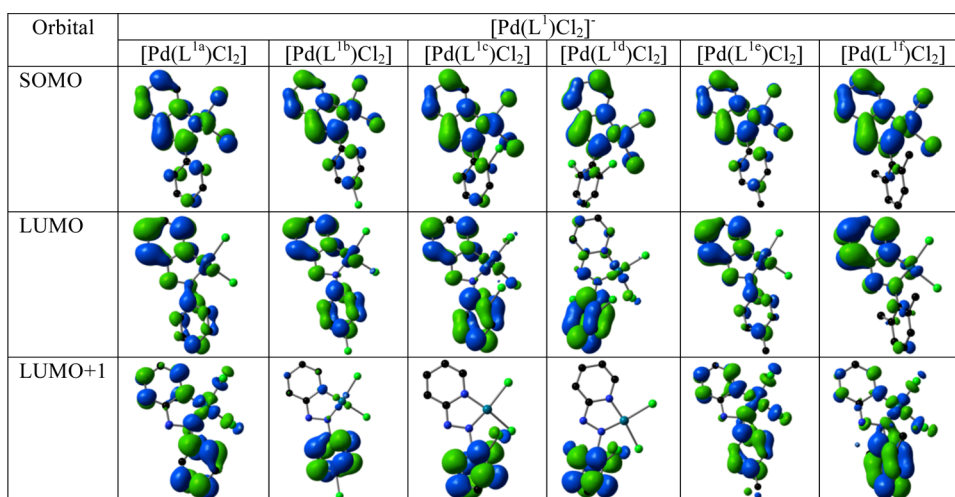


Figure 9. Associated orbitals for SOMO → LUMO transitions.

smaller and larger energy differences between the SOMO and LUMO/LUMO+1 in case of electron-withdrawing and electron-donating substituents on the pendent aryl ring, respectively (Figure 8). Notably, localization of LUMO and LUMO+1 on the pendent aryl ring suggests the distinct possibility of reduction of this aryl ring. The smaller the difference in energy between SOMO and LUMO/LUMO+1, the better the reducibility of the aryl ring is. Note here that such reduction of the pendent aryl ring is essential for the aforementioned C–N bond formation reaction. Though it was not possible to isolate the one-electron reduced pendent aryl ring containing intermediate complex, we, however, were successful in isolating another compound from a similar reduction reaction in the presence of triphenylphosphine. After its isolation and characterization by X-ray structure determination, it was found that the pendant aryl ring is metalated in the complex (Scheme 6 and Figure 7). Such metalation upon azo-reduction goes parallel to our idea of electron transfer from π^* -azo to π^* -orbital of pendant aryl ring of the ligand L¹. Thus, we propose that electron transfer to the aryl ring followed by H[•] (Cl[•]) elimination reaction from the reduced complexes is the key step for this unusual reaction. It may be noted that without ligand reduction no such *ortho*-

metalation reaction of the pendent aryl ring of ligands L¹ is possible. Moreover, a comparison of the rate of reaction with differently substituted ligands shows a good correlation with the energy difference between the SOMO and LUMO/LUMO+1, reflecting the effect of ligand substituents on the pendent aryl ring of the ligand L¹ (Figure 8). Associated molecular orbitals are also shown in Figure 9.

Moreover a prerequisite that for any bond formation reaction is that the two bond-forming atoms should be close. Thus, the scenario of an *ortho*-metalation intermediate followed by reductive elimination of H₂/HCl/alkane/alkyl halide depending upon the ligand substitution and a C–N bond formation reaction resulted the one-electron reduced azo-anion radical ligand containing product as shown in Scheme 5. Given the above experimental finding we strongly believe that this reaction pathway is a reasonable explanation of the observed chemical reaction.²⁴ Moreover, *ortho*-metalation of the phenyl ring in Pd-complexes is well-documented²⁵ in the literature. Notably, reaction with primary amine loses a proton (NH) and undergoes oxidation to result in the nonradical mono anionic ligand coordinated to a palladium(II) center.

CONCLUSIONS

To conclude, in this report we have disclosed an unusual *ortho*-C–N bond-forming reactivity of amines at the pendent aryl ring of coordinated azo-aromatic ligands L^1 in their palladium complexes. The reaction is successful for a large number of aliphatic and aromatic amines including 1°, 2°, and 3° amines. Detailed investigation shows that initial azo reduction associated with π^* -azo to π^* -aryl electron transfer initiates the C–N bond fusion reaction. The reaction has resulted in a series of palladium(II) complexes with a new redox non-innocent azo-anion radical ligands. The complexes have been characterized thoroughly by X-ray crystal structure determination, EPR, cyclic voltammetry, solution-state magnetic properties studies, and finally by DFT calculations. Variable-temperature magnetic studies of the representative complex **1c** show a relatively strong ($J = -40 \text{ cm}^{-1}$) magnetic interaction between ligand radical centers. A comparison of the redox features of the palladium complex containing a neutral NNN donor ligand to that of the mono-anionic ligand shows that the neutral NNN donor is a far more redox-active. Thus, the isolated Pd-complexes (**1a–h**) display two voltammetric waves due to redox events at the coordinated ligand. As an outcome of the interplay of redox dynamics, this genre of systems may turn out to be unique in Pd-catalyzed bond formation reactions without using any metal-based redox events. Our investigations in this area are continuing.

EXPERIMENTAL SECTION

(i). **Materials.** PdCl₂ was purchased from Arora-Matthey Limited. All other reagents and chemicals were purchased from commercial sources and used without further purifications. Solvents are dried and deoxygenated prior to use. Tetrabutylammonium perchlorate was prepared and recrystallized as reported earlier.²⁶ **Caution!** Perchlorates have to be handled with care and appropriate safety precautions.

(ii). **Physical Measurements.** A PerkinElmer Lambda 950 spectrophotometer was used to record UV–vis spectra. Infrared spectra were obtained using a PerkinElmer 783 spectrophotometer. ¹H NMR spectra were recorded on a Bruker Avance 300, 400, or 500 MHz spectrometer, and SiMe₄ was used as the internal standard. A PerkinElmer 240C elemental analyzer was used to collect micro-analytical data (C, H, N). ESI mass spectra were recorded on a micro mass Q-TOF mass spectrometer (serial no. YA 263). All electrochemical measurements were performed using a PC-controlled PAR model 273A electrochemistry system. Cyclic voltammetric experiments were performed under nitrogen atmosphere using a Ag/AgCl reference electrode, with a Pt disk working electrode and a Pt wire auxiliary electrode either in dichloromethane (**1a–h**) or in acetonitrile [Pd(L^{1a–1f})Cl₂] solution containing supporting electrolyte, 0.1 M Bu₄NClO₄. A Pt wire gauge working electrode was used for exhaustive electrolyses. $E_{1/2}$ for the ferrocenium-ferrocene couple under our experimental conditions was 0.39 V. X-band EPR spectra were recorded with a JEOL JES-FA200 spectrometer.

(iii). **Synthesis.** The ligands L^{1a–1f} were prepared by following the reported procedure.²⁷ Also complexes [Pd(L^{1a–1f})Cl₂] were prepared and characterized by following the reported procedure.^{11a}

Synthesis of [Pd(L²)Cl]1**.** All the reactions were performed following a general procedure. A mixture of [Pd(L¹)Cl₂] (1.0 equiv), the respective primary/secondary/tertiary amine (1.0 equiv), and cobaltocene (1.0 equiv) in methanol (10 mL) was heated at 300–323 K (depending on the ligand substitution) in argon-filled Schlenk line for 0.5–1.5 h. The crude product, thus obtained, was purified on a preparative alumina thin-layer chromatography plate using dichloromethane–hexane (1:50) mixture as eluent. The isolated yields and characterization of the products were as follows:

[Pd(L^{2a})Cl]**1a**. Blue colored solid. Yield: 72%. Anal. Calcd for C₁₃H₁₄ClN₄Pd: C, 42.41; H, 3.83; N, 15.22. Found C, 42.35; H, 3.81;

N, 15.20%. UV–vis (CH₂Cl₂): λ [nm] (ϵ , M⁻¹ cm⁻¹) = 272(9455), 350(13 290), 369sh(12 730), 387sh(12 040), 533sh(4950) 552(5470), 583(5420), 602sh(4050), 643(4520).

[Pd(L^{2b})Cl]**1b**. Blue colored solid. Yield: 73%. Anal. Calcd for C₁₅H₁₈ClN₄Pd: C, 45.47; H, 4.58; N, 14.14. Found C, 45.44; H, 4.56; N, 14.12%. UV–vis (CH₂Cl₂): λ [nm] (ϵ , M⁻¹ cm⁻¹) = 327(13 320), 396sh(2500), 585(960), 606sh(740), 640(880).

[Pd(L^{2c})Cl]**1c**. Blue colored solid. Yield: 74%. Anal. Calcd for C₁₈H₁₆ClN₄Pd: C, 50.25; H, 3.75; N, 13.02. Found C, 50.15; H, 3.70; N, 13.00%. UV–vis (CH₂Cl₂): λ [nm] (ϵ , M⁻¹ cm⁻¹) = 293sh(6212), 409(4457), 562(4074), 641(3841), 390(3096). IR (KBr, cm⁻¹): 1303 [ν (N=N)].

[Pd(L^{2d})Cl]**1d**. Blue colored solid. Yield: 74%. Anal. Calcd for C₁₃H₁₃Cl₂N₄Pd: C, 38.78; H, 3.25; N, 13.92. Found C, 38.73; H, 3.23; N, 13.88%. UV–vis (CH₂Cl₂): λ [nm] (ϵ , M⁻¹ cm⁻¹) = 273(7280), 289sh(7140), 338(9980), 390sh(5600), 555(2210), 583(1990), 603sh(1520), 641(1600).

[Pd(L^{2e})Cl]**1e**. Blue colored solid. Yield: 75%. Anal. Calcd for C₁₅H₁₇Cl₂N₄Pd: C, 41.83; H, 3.98; N, 13.01. Found C, 41.80; H, 3.95; N, 12.97%. UV–vis (CH₂Cl₂): λ [nm] (ϵ , M⁻¹ cm⁻¹) = 273(10 320), 355(13 150), 390sh(10 620), 528sh(4470) 548sh(4780), 576(5250), 595sh(8300), 632(4140).

[Pd(L^{2f})Cl]**1f**. Blue colored solid. Yield: 76%. Anal. Calcd for C₁₈H₁₅Cl₂N₄Pd: C, 46.53; H, 3.25; N, 12.06. Found C, 46.50; H, 3.24; N, 12.04%. UV–vis (CH₂Cl₂): λ [nm] (ϵ , M⁻¹ cm⁻¹) = 248(1700), 346(8780), 368sh(8090), 393(8000), 532sh(4140), 577(4780), 601sh(4190), 637(3880), 690(1440).

[Pd(L^{2g})Cl]**1g**. Blue colored solid. Yield: 78%. Anal. Calcd for C₂₃H₁₇Cl₂N₄Pd: C, 52.45; H, 3.25; N, 10.64. Found C, 52.40; H, 3.23; N, 10.60%. UV–vis (CH₂Cl₂): λ [nm] (ϵ , M⁻¹ cm⁻¹) = 346(1770), 379sh(14 180), 517sh(5810), 537sh(6250), 566(7280), 584sh(5560), 623(5470).

[Pd(L^{2h})Cl]**1h**. Blue colored solid. Yield: 72%. Anal. Calcd for C₁₃H₁₃Cl₂N₄Pd: C, 38.78; H, 3.25; N, 13.92. Found C, 38.69; H, 3.20; N, 13.88%. UV–vis (CH₂Cl₂): λ [nm] (ϵ , M⁻¹ cm⁻¹) = 277(6030), 351(7610), 583(2770), 640(2080).

Nuclear Magnetic Resonance Spectrum of Oxidized Complex [1f]⁺. In an NMR tube, 20 mg (0.05 mmol) of **1f** was mixed with a slight excess (15 mg, 0.06 mmol) of iodine in 2 mL of CDCl₃ solution. The solution turned dark blue in color. The ¹H NMR spectrum of the crude oxidized product was recorded instantaneously. The ¹H NMR spectrum is given below:

[1f]⁺. ¹H NMR (500 MHz, CDCl₃) δ 7.702 (d, $J = 6$ Hz), δ 7.537 (t, $J = 8$ Hz), δ 7.453–7.406 (m), δ 7.353–7.311 (m), δ 7.250, δ 7.200 (d, $J = 7.5$ Hz), δ 6.996 (t, $J = 8$ Hz), δ 6.810 (d, $J = 8$ Hz), δ 6.588 (d, $J = 7$ Hz).

(iv). **X-ray Crystallography.** Crystallographic data for complexes **1c**, **1e**, **1f**, **1h**, and Pd–I are collected in Table S5. Suitable X-ray quality crystals of these complexes are obtained either by the slow evaporation of a dichloromethane–hexane solution of the complex or slow diffusion of a dichloromethane solution of the complex into hexane. All data were collected on a Bruker SMART APEX-II diffractometer, equipped with graphite-monochromated Mo $K\alpha$ radiation ($\lambda = 0.710 73 \text{ \AA}$) and were corrected for Lorentz polarization effects. **1c**: A total of 21 535 reflections were collected, of which 3760 were unique ($R_{\text{int}} = 0.025$). **1e**: A total of 14 342 reflections were collected, of which 3715 were unique ($R_{\text{int}} = 0.024$), satisfying the $I > 2\sigma(I)$ criterion, and were used in subsequent analysis. **1f**: A total of 100 094 reflections were collected, of which 2962 were unique ($R_{\text{int}} = 0.089$). **1h**: A total of 18 681 reflections were collected, of which 5784 were unique ($R_{\text{int}} = 0.039$). Pd–I: A total of 16 587 reflections were collected, of which 5724 were unique ($R_{\text{int}} = 0.083$). The structures were solved by employing the SHELXS-2013 program package and were refined by full-matrix least-squares based on F^2 (SHELXL-2013).²⁸ All hydrogen atoms were added in calculated positions.

(v). **Solution-State Magnetic Susceptibility Measurement by Evans Method.** Magnetic susceptibility measurements for the isolated species **1c**, **1e**, **1f**, and **1g** were made by Evans method²⁹ with a Bruker Avance 500 MHz spectrometer at 300 K. The solution

magnetic susceptibility was determined by using the following equation:

$$\chi_g = \frac{-3\Delta f}{4\pi Fm} + \chi_D$$

where χ_g is the gram susceptibility of the solvent in $\text{cm}^3 \text{g}^{-1}$, Δf is the chemical shift difference (in Hz) between a reference proton in the sample and that in a solution lacking the paramagnetic compound, F is the fixed probe frequency of the spectrometer, m is the mass of the complex in grams in 1 cm^3 of solution, and χ_D is the diamagnetic susceptibility. The corrections for the susceptibility of the solvent and the difference in densities of the solvent and the solution are ignored.³⁰

The diamagnetic correction to the molar susceptibility χ_m was calculated from Pascal's constants,³¹ and the effective magnetic moment μ_{eff} was calculated by using the standard equation, where χ_m is the corrected molar susceptibility and T is the temperature in K.

$$\mu_{\text{eff}} = 2.828(\chi_m T)^{1/2} (\mu_B)$$

(vi). SQUID Magnetic Susceptibility Measurements of Solid Material. Temperature-dependent magnetic susceptibility measurements for **1c** were performed with a Quantum-Design MPMS-XL-5 SQUID magnetometer equipped with a 5 T magnet in the range from 295 to 2.0 K at a magnetic field of 0.5 T. The powdered sample was contained in a gelatin capsule and fixed in a nonmagnetic sample holder. Each raw data file for the measured magnetic moment was corrected for the diamagnetic contribution of the gelatin capsule according to $M^{\text{dia}}(\text{capsule}) = \chi_g \cdot m \cdot H$, with an experimentally obtained gram susceptibility of the gelatin capsule. The molar susceptibility data were corrected for the diamagnetic contribution using the Pascal constants and the increment method according to Haberdtz.³² The experimental data were fitted using the appropriate Heisenberg–Dirac–van Vleck spin Hamiltonian that includes the isotropic exchange coupling constant and Zeeman splitting (see eq 1 in the main text).³³ Temperature-independent paramagnetism (TIP) and paramagnetic impurities (PI) were included according to $\chi_{\text{calc}} = (1 - \text{PI}) \cdot \chi + \text{TIP}$ (TIP = $20 \times 10^{-6} \text{ cm}^3 \text{mol}^{-1}$, PI = 5% (per one molecule of **1c**, fixed value)). Intermolecular interactions were considered in a mean field approach by using a Weiss temperature Θ .³⁴ The Weiss temperature $\Theta = -15.2 \text{ K}$ (defined as $\Theta = zJS(S+1)/3k$) relates to intermolecular interactions zJ of -42.3 cm^{-1} for **1c**, where J is the interaction parameter between two nearest neighbor magnetic centers, k is the Boltzmann constant ($0.695 \text{ cm}^{-1} \cdot \text{K}^{-1}$), and z is the number of nearest neighbors.

■ ASSOCIATED CONTENT

Supporting Information

The Supporting Information is available free of charge on the ACS Publications website at DOI: 10.1021/acs.inorgchem.5b02110.

Figures and tables giving crystallographic details and selected bond parameters of the complexes **1c**, **1e**, **1f**, **1h**, and **Pd–I**, relevant cyclic voltammograms, spectral data, ORTEP representations, contour plots and Cartesian coordinates of the optimized structures. (PDF) Additional crystallographic details. (CIF)

■ AUTHOR INFORMATION

Corresponding Author

*E-mail: icsg@iacs.res.in.

Notes

The authors declare no competing financial interest.

■ ACKNOWLEDGMENTS

The research was supported by the Department of Science and Technology (DST), India, and Council of Scientific and Industrial Research (CSIR) funded projects, SR/S2/JCB-09/

2011 and 01(274)/13/EMR-II, respectively. S.G. sincerely thanks DST for a J. C. Bose fellowship. D.S. and P.G. are thankful to the CSIR for their fellowship support. S.S. is thankful to the DST inspire fellowship support. Crystallography was performed at the DST-funded National Single Crystal Diffractometer facility at the Department of Inorganic Chemistry, IACS. We thank Prof. S. Bhattacharya of Jadavpur Univ. for GC-MS analysis.

■ DEDICATION

Dedicated to Professor Animesh Chakravorty on his 80th birth anniversary.

■ REFERENCES

- (1) (a) Chirik, P. J.; Wieghardt, K. *Science* **2010**, *327*, 794–795. (b) Dzik, W. I.; van der Vlugt, J. I.; Reek, J. N. H.; de Bruin, B. *Angew. Chem., Int. Ed.* **2011**, *50*, 3356–3358. (c) Lyaskovskyy, V.; de Bruin, B. *ACS Catal.* **2012**, *2*, 270–279. (d) Gruetzmacher, H. *Angew. Chem., Int. Ed.* **2008**, *47*, 1814–1818. (e) Chirik, P. J. *Inorg. Chem.* **2011**, *50*, 9737–9740. (f) Kaim, W. *Eur. J. Inorg. Chem.* **2012**, *2012*, 343–348.
- (2) (a) Kaim, W.; Schwederski, B. *Coord. Chem. Rev.* **2010**, *254*, 1580–1588. (b) Kaim, W. *Dalton Trans.* **2003**, 761–768.
- (3) (a) Vickers, E. B.; Giles, I. D.; Miller, J. S. *Chem. Mater.* **2005**, *17*, 1667–1672. (b) Wang, Z.-X.; Zhang, X.; Zhang, Y.-Z.; Li, M.-X.; Zhao, H.; Andruh, M.; Dunbar, K. R. *Angew. Chem., Int. Ed.* **2014**, *53*, 11567–11570.
- (4) (a) Goswami, S.; Sengupta, D.; Paul, N. D.; Mondal, T. K.; Goswami, S. *Chem. - Eur. J.* **2014**, *20*, 6103–6111. (b) Paul, N. D.; Rana, U.; Goswami, S.; Mondal, T. K.; Goswami, S. *J. Am. Chem. Soc.* **2012**, *134*, 6520–6523.
- (5) (a) Praneeth, V. K. K.; Ringenberg, M. R.; Ward, T. R. *Angew. Chem., Int. Ed.* **2012**, *51*, 10228–10234. (b) Luca, O. R.; Crabtree, R. H. *Chem. Soc. Rev.* **2013**, *42*, 1440–1459.
- (6) (a) Russell, S. K.; Lobkovsky, E.; Chirik, P. J. *J. Am. Chem. Soc.* **2011**, *133*, 8858–8861. (b) Monfette, S.; Turner, Z. R.; Semproni, S. P.; Chirik, P. J. *J. Am. Chem. Soc.* **2012**, *134*, 4561–4564. (c) Darmon, J. M.; Stieber, S. C. E.; Sylvester, K. T.; Fernandez, I.; Lobkovsky, E.; Semproni, S. P.; Bill, E.; Wieghardt, K.; DeBeer, S.; Chirik, P. J. *J. Am. Chem. Soc.* **2012**, *134*, 17125–17137.
- (7) Broere, D. L. J.; de Bruin, B.; Reek, J. N. H.; Lutz, M.; Dechert, S.; van der Vlugt, J. I. *J. Am. Chem. Soc.* **2014**, *136*, 11574–11577.
- (8) Hall, G. B.; Kottani, R.; Felton, G. A. N.; Yamamoto, T.; Evans, D. H.; Glass, R. S.; Lichtenberger, D. L. *J. Am. Chem. Soc.* **2014**, *136*, 4012–4018.
- (9) (a) Sanyal, A.; Chatterjee, S.; Castineiras, A.; Sarkar, B.; Singh, P.; Fiedler, J.; Zalis, S.; Kaim, W.; Goswami, S. *Inorg. Chem.* **2007**, *46*, 8584–8593. (b) Saha, A.; Ghosh, A. K.; Majumdar, P.; Mitra, K. N.; Mondal, S.; Rajak, K. K.; Falvello, L. R.; Goswami, S. *Organometallics* **1999**, *18*, 3772–3774.
- (10) (a) Johnston, C. W.; McKinnon, S. D. J.; Patrick, B. O.; Hicks, R. G. *Dalton Trans.* **2013**, *42*, 16829–16836. (b) Sanz, C. A.; Ferguson, M. J.; McDonald, R.; Patrick, B. O.; Hicks, R. G. *Chem. Commun.* **2014**, *50*, 11676–11678.
- (11) (a) Roy, S.; Hartenbach, I.; Sarkar, B. *Eur. J. Inorg. Chem.* **2009**, *2009*, 2553–2558. (b) Sinha, C. Ph. D. Thesis, Jadavpur University, 1990.
- (12) Kamar, K. K.; Das, S.; Hung, C.-H.; Castineiras, A.; Kuz'min, M. D.; Rillo, C.; Bartolome, J.; Goswami, S. *Inorg. Chem.* **2003**, *42*, 5367–5375.
- (13) Samanta, S.; Ghosh, P.; Goswami, S. *Dalton Trans.* **2012**, *41*, 2213–2226.
- (14) (a) Desiraju, G. R.; Steiner, T. *The Weak Hydrogen Bond In Structural Chemistry and Biology*; Oxford University Press, 1999. (b) Bhogala, B. R.; Nangia, A. *Cryst. Growth Des.* **2003**, *3*, 547–554. (c) Janiak, C. *Dalton Trans.* **2000**, 3885–3896. (d) Nishio, M. *CrystEngComm* **2004**, *6*, 130–158. (e) Seth, S. K. *J. Mol. Struct.* **2014**,

1070, 65–74. (f) Seth, S. K.; Sarkar, D.; Roy, A.; Kar, T. *CrystEngComm* **2011**, *13*, 6728–6741.

(15) (a) Seth, S. K.; Sarkar, D.; Kar, T. *CrystEngComm* **2011**, *13*, 4528–4535. (b) Seth, S. K. *CrystEngComm* **2013**, *15*, 1772–1781.

(16) (a) Koivisto, B. D.; Ichimura, A. S.; McDonald, R.; Lemaire, M. T.; Thompson, L. K.; Hicks, R. G. *J. Am. Chem. Soc.* **2006**, *128*, 690–691. (b) Chi, Y.-H.; Shi, J.-M.; Li, H.-N.; Wei, W.; Cottrill, E.; Pan, N.; Chen, H.; Liang, Y.; Yu, L.; Zhang, Y.-Q.; Hou, C. *Dalton Trans.* **2013**, *42*, 15559–15569.

(17) (a) Hicks, R. G.; Lemaire, M. T.; Oehrstroem, L.; Richardson, J. F.; Thompson, L. K.; Xu, Z. *J. Am. Chem. Soc.* **2001**, *123*, 7154–7159. (b) Pal, S. K.; Itkis, M. E.; Reed, R. W.; Oakley, R. T.; Cordes, A. W.; Tham, F. S.; Siegrist, T.; Haddon, R. C. *J. Am. Chem. Soc.* **2004**, *126*, 1478–1484.

(18) Chakraborty, I.; Panda, B. K.; Gangopadhyay, J.; Chakravorty, A. *Inorg. Chem.* **2005**, *44*, 1054–1060.

(19) Cope, A. C.; Siekman, R. W. *J. Am. Chem. Soc.* **1965**, *87*, 3272–3.

(20) Widger, L. R.; Jiang, Y.; Siegler, M. A.; Kumar, D.; Latifi, R.; de Visser, S. P.; Jameson, G. N. L.; Goldberg, D. P. *Inorg. Chem.* **2013**, *52*, 10467–10480.

(21) Blonski, C.; Myers, A. W.; Palmer, M.; Harris, S.; Jones, W. D. *Organometallics* **1997**, *16*, 3819–3827.

(22) Pfeiffer, M. G.; Schaefer, B.; Smolentsev, G.; Uhlig, J.; Nazarenko, E.; Guthmuller, J.; Kuhnt, C.; Waechtler, M.; Dietzek, B.; Sundstroem, V.; Rau, S. *Angew. Chem., Int. Ed.* **2015**, *54*, 5044–5048.

(23) Ghosh, P.; Samanta, S.; Roy, S. K.; Demeshko, S.; Meyer, F.; Goswami, S. *Inorg. Chem.* **2014**, *53*, 4678–4686.

(24) (a) Dimmer, J.-A.; Hornung, M.; Wuetz, T.; Wesemann, L. *Organometallics* **2012**, *31*, 7044–7051. (b) Kumar, S.; Mani, G.; Mondal, S.; Chattaraj, P. K. *Inorg. Chem.* **2012**, *51*, 12527–12539.

(25) Khare, G. P.; Little, R. G.; Veal, J. T.; Doedens, R. J. *Inorg. Chem.* **1975**, *14*, 2475–9.

(26) Goswami, S.; Mukherjee, R.; Chakravorty, A. *Inorg. Chem.* **1983**, *22*, 2825–32.

(27) Ghosh, P.; Samanta, S.; Roy, S. K.; Joy, S.; Kramer, T.; McGrady, J. E.; Goswami, S. *Inorg. Chem.* **2013**, *52*, 14040–14049.

(28) Sheldrick, G. M. *Acta Crystallogr., Sect. A: Found. Crystallogr.* **2008**, *64*, 112–122.

(29) (a) Evans, D. F. *J. Chem. Soc.* **1959**, 2003–5. (b) Naklicki, M. L.; White, C. A.; Plante, L. L.; Evans, C. E. B.; Crutchley, R. J. *Inorg. Chem.* **1998**, *37*, 1880–1885. (c) Casabianca, L. B.; An, D.; Natarajan, J. K.; Alumasa, J. N.; Roepe, P. D.; Wolf, C.; de Dios, A. C. *Inorg. Chem.* **2008**, *47*, 6077–6081.

(30) Weast, R. C. *CRC Handbook of Chemistry and Physics*; CRC Press, 1980; Vol. 60.

(31) Drago, R. S. *Physical methods for chemists*, 2nd ed.; Saunders College Publishing: Philadelphia, PA, 1992.

(32) Haberditzl, W. *Angew. Chem., Int. Ed. Engl.* **1966**, *5*, 288–98.

(33) Simulation of the experimental magnetic data was performed with the *julX* program (Bill, E. Max-Planck Institute for Chemical Energy Conversion: Mülheim/Ruhr, Germany).

(34) Kahn, O. *Molecular Magnetism*; VCH, Weinheim, 1993.